Polarized exocytosis and anionic phospholipid species implicated in the initiation of clathrin-mediated endocytosis

Paul Marchando, Gean Hu, Yidi Sun, David G. Drubin*

16 Barker Hall, Dept. of Molecular and Cell Biology, University of California, Berkeley, CA 94720, USA.

* Corresponding author

phone: 510-642-3692, fax: 510-643-0062,
e-mail: drubin@berkeley.edu

Abstract

Understanding of the mechanisms that initiate clathrin-mediated endocytosis (CME) is incomplete. Recent studies in budding yeast identified the endocytic adaptor protein Yap1801/Yap1802 (budding yeast AP180) as a key CME factor that promotes CME initiation in daughter cells during polarized growth, but how Yap1801/2 is recruited preferentially to the plasma membrane of daughter cells is not clear. The only known cargos for Yap1801/2 in yeast are the synaptobrevins Snc1 and Snc2, which act as v-SNARES for exocytic vesicles arriving at the plasma membrane and are essential for polarized cell growth. In this study, we analyze the spatiotemporal dynamics of functional, fluorescently-tagged Snc1/2 expressed from their endogenous loci and provide evidence that, in concert with anionic phospholipids, Snc1/2 recruit Yap1801/2 preferentially to growing daughter cells. These findings suggest that the coincidence of anionic phospholipids and Snc1/2 facilitates CME initiation in growing daughter cells and directly links polarized CME to polarized secretion.

Introduction

While much research has focused on how clathrin-mediated endocytosis (CME) is initiated, consensus about the molecular mechanism has not been reached (Godlee and Kaksonen, 2013). Rab GTPases are known to initiate many trafficking processes, but no single trigger or pioneering factor for CME has been identified (Kreis *et al.*, 1995; Godlee and Kaksonen, 2013; Martin and Arkowitz, 2014), although membrane-bound cargo has been proposed to play a role (Taylor *et al.*, 2011; Goode *et al.*, 2015; Pedersen *et al.*, 2020).

In the budding yeast *Saccharomyces cerevisiae*, recent studies demonstrated that CME site initiation and maturation dynamics depend on position on the plasma membrane within a growing, polarized yeast cell (Layton *et al.*, 2011; Pedersen *et al.*, 2020; Sun *et al.*, 2024). Budding yeast proliferate by forming daughter cells, also referred to as “buds,” on the surface of a mother cell. Exocytosis is highly biased toward the daughter cell, so molecules delivered to the plasma membrane during exocytosis, such as SNARE proteins, are enriched near these exocytic sites (Field and Schekman, 1980). Since CME is the major pathway that retrieves material from

the plasma membrane back into the cell interior, the presence of cargo concentrated in the bud might affect CME site initiation or maturation (Carroll *et al.*, 2012; Cocucci *et al.*, 2012; Brach *et al.*, 2014). Indirect approaches have supported this possibility, but a direct link between polarized secretion and polarized CME (originally observed as polarized actin patches) has yet to be demonstrated (Adams and Pringle, 1984; Goode *et al.*, 2015; Pedersen *et al.*, 2020).

CME in budding yeast displays two temporal phases with distinct behaviors (Pedersen *et al.*, 2020). The transition between these phases coincides with differential Pan1 (budding yeast intersectin homolog) behavior in mother and daughter cells (Sun *et al.*, 2024). Pan1 undergoes a "low-abundance" phase followed by a "high-abundance" phase in mother cells, while only displaying the high-abundance phase in daughters (Sun *et al.*, 2024). We thus define early-arriving proteins as those that appear at CME sites before the high-abundance Pan1 phase, and late-arriving proteins as those that appear during or after the high-abundance Pan1 phase (Brach *et al.*, 2014; Bradford *et al.*, 2015; Sun *et al.*, 2015, 2017, 2024; Pedersen *et al.*, 2020). Early-arriving proteins show position-dependent differences in lifetimes (short and regular in daughters, longer and variable in mothers), while late-arriving proteins exhibit more regular lifetimes regardless of cell growth stage or position within the cell (Pedersen *et al.*, 2020; Sun *et al.*, 2024).

This heterogeneity in CME site behavior is partly driven by the endocytic adaptor complex AP180 (Yap1801 and Yap1802 in yeast, abbreviated as Yap1801/2) (Sun *et al.*, 2024). Yap1801/2 interact cooperatively with the FCHo1/2 homolog Syp1 to recruit the EPS15 homolog Ede1 to the bud cortex, initiating the early stages of CME (Lu and Drubin, 2017; Sun *et al.*, 2024). Yap1801/2 are polarized strongly to the bud during yeast cell growth while mother cells, have nearly undetectable Yap1801/2, explaining the observed position-dependent differences in CME initiation rates and lifetimes (Sun *et al.*, 2024). While Yap1801/2's role in CME initiation as perhaps the earliest acting factor is more clear, the factors upstream of Yap1801/2 recruitment remain speculative (Sun *et al.*, 2024).

Yap1801/2 have one known cargo, the v-SNAREs Snc1 and Snc2 (abbreviated as Snc1/2), homologs of the mammalian synaptobrevins, which depend of CME for their retrieval from the plasma membrane (Burston *et al.*, 2009; Miller *et al.*, 2011). Snc1/2 are the only known v-SNAREs in budding yeast that facilitate the fusion of secretory vesicles with the plasma membrane (Burri and Lithgow, 2004). In addition to binding Snc1/2, Yap1801/2 can directly bind anionic lipid species (Ford *et al.*, 2001). Since both Snc1/2 and anionic lipid species, particularly phosphatidylserine, are enriched in daughter cells, Snc1/2 and anionic lipids are poised to play a role in the asymmetrical behavior of Yap1801/2 in yeast undergoing bud growth (Burston *et al.*, 2009; Sun and Drubin, 2012; Meca *et al.*, 2019). The residues in Yap1801/2 mediating both binding activities are well characterized, and precise perturbation of both Snc1/2 and lipid binding could reveal if both are equally important for Yap1802 recruitment or if one overshadows the other.

The yeast synaptobrevins Snc1/2 thus provide a unique opportunity to study the earliest stages of CME and better characterize a yeast CME cargo, a task that has remained difficult and yielded

mixed results in past studies (Toshima *et al.*, 2006; Carroll *et al.*, 2009). Here, using high-resolution live-cell microscopy, we provide the first spatiotemporal characterization of Snc1 and Snc2 expressed from their endogenous promoters at their chromosomal loci, highlighting a complex relationship with CME that depends on cell growth stage. Further experiments show that Snc1/2 and anionic phospholipids together facilitate CME initiation by recruiting the endocytic adaptors Yap1801/2 to daughter cells during cell growth.

Results and Discussion

Functional GFP-tagged Snc1 and Snc2 fusion proteins expressed from their endogenous genomic loci display complex spatiotemporal behaviors relative to the CME machinery

To analyze the spatial distribution of Snc1 and Snc2 in yeast cells, we created in-frame fusions of the corresponding genes at their endogenous genomic loci with sequences encoding GFP and visualized the N-terminally-tagged fluorescent fusion proteins in cells by Airyscan (Zeiss) confocal microscopy (Figure 1A). The two proteins displayed similar subcellular localization, appearing preferentially at the plasma membrane of growing daughter cells, in agreement with previous studies of overexpressed Snc1, and they both decorated internal structures that presumably are membrane-bound organelles (Burston *et al.*, 2009). The GFP-Snc1 fusions displayed weak signals, consistent with the low signal observed on immunoblots, suggesting a greater abundance of Snc2 (Figure S1A). In addition, *snc2Δ* strains were more severely impaired in growth than *snc1Δ* strains (Figure S1B, G). Even though Snc1/2 display 76% sequence identity (Katz *et al.*, 1998), *SNC2* transcripts outnumber *SNC1* transcripts nearly threefold, perhaps explaining the differential behaviors (Grote *et al.*, 2000; Gurunathan *et al.*, 2000; Lipson *et al.*, 2009). Due to the greater abundance and importance for cell growth of Snc2, we focus on GFP-Snc2 henceforth. Since GFP-Snc2 expressed from the endogenous promoter was able to rescue the growth defects of *snc2*Δ cells, we conclude that this fusion protein is functional and likely to serve as a faithful reporter of the spatiotemporal dynamics of these v-SNARES (Figure S1B, G).

We next studied the complex behaviors and interactions of Snc2 with the CME machinery (reported by Sla1-mScarlet) in live cells using Nikon Spatial Array Confocal (NSPARC) microscopy at sub-second temporal resolution (Supplemental Videos 1 and 2) (Delattre, 2023). Snc2 and Sla1 both showed preferential localization to the plasma membrane in daughter cells, but Snc2 was largely diffuse on the plasma membrane while Sla1 was punctate (Figure 1B). In these daughter cells, the most clearly observable Snc2 behavior resembled that observed for early endosomes labeled with fluorescent alpha factor (Toshima *et al.*, 2006) and the lipophilic dye FM 4-64 (Cortesio *et al.*, 2015) in our earlier studies. Bright Snc2-positive compartments, possibly early endosomes, translated across large lengths of budded cells in several seconds, and appeared to move from one endocytic site to another at the daughter cell cortex in a coordinated manner (Figure 1C, white arrows, Supplemental Videos 1 and 2, arrows). While erratic, this “vacuum cleaner” behavior, in which Snc2 structures appear move to Sla1 sites as if collecting vesicles as they bud from the membrane, suggests a high level of spatial and temporal coordination between Snc2-labeled cytoplasmic structures and internalizing CME sites. Additionally, punctate cytoplasmic structures moved directionally from mother cells toward daughter cells, consistent with their participation in polarized secretion (Figure 1C, yellow arrows, Supplemental Video 1, arrows).

Using circumferential kymographs created by tracing the outline of the plasma membrane on the vertical axis and projecting the outline through time on the horizontal axis, we better observed how Snc2-positive compartments interact with the plasma membrane in mother vs. daughter cells (Figure 1D) (Lu and Drubin, 2017; Sun *et al.*, 2017). In daughter cells, GFP-Snc2

appeared on the plasma membrane diffusely, and bright traces of Snc2-positive compartments undergoing "vacuum cleaner" behavior interacted transiently with the plasma membrane and overlapped with Sla1 traces (Figure 1D, white arrows). In traces from mother cells, Snc2 puncta translated laterally across the plasma membrane, occasionally coinciding with the internalization of endocytic vesicles (Figure 1D, yellow arrows). Unbudded cells displayed a mixture of these behaviors, with brighter traces that fluctuate less in intensity and show longer lifetimes (Figure 1D, third row). On rare occasions, Snc2-positive punctate traces were observed to track and disappear with Sla1 in a manner consistent with CME cargo behavior (Figure 1D, cyan arrows).

While Snc1/2 have well-established roles in the exocytic fusion of vesicles formed at the trans-Golgi network (TGN) with the plasma membrane, previous studies have suggested that these proteins might also play a role in the fusion of early endosomes with the TGN (Gurunathan *et al.*, 2000; Lewis *et al.*, 2000; Burri and Lithgow, 2004; Best *et al.*, 2020). Our observations are consistent with a possible additional function for Snc2-positive compartments that appear to interact with the plasma membrane transiently. These events could represent endosomes that fuse with nascent endocytic vesicles via the action of these SNARE proteins, but whether SNARE function plays an active role in this behavior remains to be investigated.

Snc1/2 internalization from the cell surface via CME is important for cell viability

CME perturbation highlights a clear dependency of Snc2 on CME for internalization. Treatment of yeast cells with the Arp2/3 complex inhibitor CK-666 halted endocytic internalization (Hetrick *et al.*, 2013) and trapped Snc2 preferentially on the plasma membrane in daughter cells while Snc2 cytoplasmic puncta disappeared (Figure 1E). In these cells, stalled endocytic sites, marked by Sla1-mScarlet, appeared as stationary puncta on the plasma membrane, although Snc2 signal was not noticeably enriched at these puncta. Upon CK-666 washout, Snc2 could again be seen on cytoplasmic puncta and appeared brighter, perhaps due to the drug-induced local Snc2 enrichment in daughter cells (Figure 1E). This observation suggests that Snc2 behaves differently from core components of the endocytic machinery, which form puncta that colocalize at CME sites and track with internalizing vesicles. Observing cargo associated with CME sites is notoriously difficult due to signal-to-noise challenges as cargo saturate CME sites and accumulate on the plasma membrane.

Previous work on the mammalian synaptobrevins identified residues that mediate their interaction with the endocytic adapter CALM, a mammalian homolog of Yap1801/2 (Grote *et al.*, 2000; Gurunathan *et al.*, 2000; Miller *et al.*, 2011). The residues important for this interaction correspond to V39 and M42 on Snc2. Alanine substitutions at these residues did not affect Snc2 expression (Figure S1C) but resulted in diffuse Snc2 signal on the plasma membrane in both daughter and mother cells (Figure 1F) (Grote *et al.*, 2000; Gurunathan *et al.*, 2000; Lewis *et al.*, 2000; Shen *et al.*, 2013). This result suggests that the V39A M42A Snc2 mutant is still competent to mediate exocytosis, Snc1/2's essential function, and that CME of Snc1 alone is sufficient for yeast to remain healthy. We tested the latter conclusion in an *snc1Δ* background, wherein the Snc2 mutant again showed diffuse plasma membrane staining in mother and

daughter cells, but these cells display a severe growth defect, irregular morphologies, and diffuse Snc2 cytoplasmic signal consistent with vacuolar fragmenting or sorting defects observed in unhealthy cells (Figure 1F, S1D, G) (Stauffer and Powers, 2015). These observations indicate that CME of some Snc1/2 molecules is essential for normal cell physiology. While it is possible that the V39A M42A mutation impacts other cellular processes in which Snc1/2 are involved, the conserved methionine residue has been shown to specifically mediate the interaction of synaptobrevins with CALM/AP180, and previous studies demonstrated that CME of SNAREs and their ability to mediate exocytosis are separable activities (Miller *et al.*, 2011; Ma and Burd, 2019).

Roles for polarized anionic phospholipid and Snc1/2 localization in polarized AP180 recruitment and CME initiation

We next created specific point mutations in Yap1802 to investigate the relationship between Snc1/2 interaction with Yap1802 and polarized CME site formation. Residues of the mammalian Yap1802 homolog CALM that mediate its interaction with anionic phospholipids and synaptobrevins have been characterized and fall within its ANTH (AP180 N-terminal homology) domain (Ford *et al.*, 2001; Miller *et al.*, 2011; Pashkova *et al.*, 2021). The analogous residues in *S. cerevisiae* Yap1802 correspond to lysines 21 and 23 for lipid interaction and leucine 203 for Snc1/2 interaction (Figure 2A-B) (Ford *et al.*, 2001; Miller *et al.*, 2011; Pashkova *et al.*, 2021). Alphafold2 multimer analysis strengthened confidence that L203 in Yap1802 interacts with M42 in Snc2 (Figure 2B) (Mirdita *et al.*, 2022). Using a CRISPR/Cas9-based approach to generate Yap1802 K21E K23E and L203S mutants, we tested whether interactions of Yap1802 with anionic phospholipids and plasma membrane-bound Snc1/2 might facilitate Yap1801/2 recruitment (Anand *et al.*, 2017). Given the high degree of homology between Yap1801 and Yap1802, the observation that Yap1802 is functionally sufficient in *yap1801Δ* cells, and the strong polarization of Yap1802 to small- and medium-sized daughter cells, we decided to conduct experiments on point-mutated Yap1802 mutants in a *yap1801Δ* background (Sun *et al.*, 2024). The mutated strains showed no detectable difference in Yap1802 expression levels and did not cause an observable temperature-sensitive cell viability defect (Figure S1E-G).

Yeast strains individually expressing the Yap1802 K21E K23E mutant (predicted to be defective in lipid binding), the Yap1802 L203S mutant (predicted to be defective in Snc1/2 binding), or the Yap1802 3x PM (K21E K23E L203S, predicted to be defective in both lipid and Snc1/2 binding) each displayed a Yap1802 recruitment defect, which can be best visualized using maximum intensity projections of timelapse movies (Figure 2C). In these projections, quantification of the mean cortex fluorescence intensity in daughter cells showed a decrease in plasma membrane Yap1802 signal among all point mutants tested (Figure 2E). Additionally, looking closer at these cortex intensity traces in daughter cells revealed a unimodal curve with a maximum near the middle of the trace, coinciding with the very tip of the growing bud (Figure S2A). Each individual mutant lost this curved Yap1802 trace and showed reduced intensity along the length of each trace. Individual Yap1802 endocytic events in budded cells were still observed in each mutant, with the lipid and Snc1/2 mutants maintaining normal lifetimes compared to cells expressing wild-type Yap1802 (Figure 2D, 2F). However, the lifetimes of Yap1802 3x PM-GFP events were

significantly shorter than those for the wild-type cells and individual mutants (Figure 2F). These 3x PM lifetimes are consistent with those observed in strains that lack the ability to localize Ede1 properly, such as *yap1801Δ/yap1802Δ* double null mutants and *ede1Δ* cells (Brach *et al.*, 2014; Sun *et al.*, 2024). We note that in Figure 2C Yap1802 3x PM-GFP shows an elevated signal at the bud neck, which is representative of the localization for this mutant. We speculate that since Yap1802 3x PM-GFP is defective in both lipid and Snc1/2 binding, it is recruited to the bud neck by Ede1 through YAP1802's NPF motifs because Ede1 is concentrated at the bud neck (Pedersen *et al.*, 2020).

Since perturbing Yap1801/2's interaction with lipids and cargo (Snc1/2) led to abnormal Yap1801/2 behavior, we investigated whether these endocytic perturbations also led to abnormal Snc2 behavior. Using confocal microscopy to visualize endogenously expressed mScarlet-Snc2 in yeast strains expressing point-mutated Yap1802-GFP fusion proteins, we observed differential distributions of Snc2 on the plasma membrane (Figure 2G). *yap1801Δ YAP1802* cells displayed normal Snc2 localization when compared to wild-type cells, but each point mutant led to defects in Snc2 internalization, with an increase in Snc2 cortex signal in mother cells across all conditions (Figure 2H, Figure S2B).

Taken together, these findings identify anionic phospholipids and Snc1/2 as important factors facilitating the initiation of CME. Since wild-type Yap1802 interacts with Snc1/2 directly and is most concentrated at the daughter cell tip where exocytosis is most active, Yap1801/2 localization is directly linked to polarized cell growth and secretion (Figure 3A). Signaling initiated by Cdc42 causes actin cable assembly from the daughter cell tip, enabling a type V myosin to recruit many cellular components, including secretory vesicles and the exocyst vesicle tethering complex to the bud tip (Figure 3A) (Pruyne and Bretscher, 2000a, 2000b; Mei and Guo, 2018; Mei *et al.*, 2018). Once vesicles reach the cortex, we suggest that Snc1/2 and anionic phospholipids act as a landing pad for the machinery that initiates CME site formation. Since Yap1801/2's lipid binding and Snc1/2 binding display roughly equal importance for Yap1801/2 recruitment, we suggest that robust Yap1801/2 localization relies on its coincidence detection of these two factors (Figure 3B).

Interestingly, we could not precisely perturb the endocytic machinery in a way that led to cell growth defects like those observed in *snc2 V39A M42A/snc1Δ* cells. Since *yap1801Δ/yap1802Δ* double null cells also display essentially normal growth and viability, this result suggests the existence of adaptor proteins in addition to Yap1801/2 that can mediate Snc1/2 internalization, perhaps AP2 or Syp1 (Sun *et al.*, 2024). In addition, the Hip1/R homolog Sla2, which also contains an ANTH domain, and the epsins Ent1 and Ent2, could be candidates for this role. However, since *sla2Δ* and *ent1Δ/ent2Δ* cells are completely defective in CME, and since our efforts to identify Sla2 or Ent1/2 residues that might mediate interactions between these proteins and Snc1/2 using Alphafold2 multimer analysis were not successful, studying the effect these proteins have on Snc1/2 internalization must await future studies and new approaches (Sun *et al.*, 2005; Maldonado-Báez *et al.*, 2008; Mirdita *et al.*, 2022).

Conclusions

Here, we provide evidence that the previously identified interactions between the endocytic adaptor AP180 and the Snc1/2 CME cargo and anionic phospholipids facilitate CME initiation in daughter cells and provide a link between polarized cell growth driven by localized exocytosis and CME. The polarized delivery of Snc1/2 to the plasma membrane by exocytosis and the subsequent endocytosis of these proteins appears to be highly coordinated, as CME sites are concentrated near sites of localized exocytosis. As the proteins investigated here are highly conserved in all eukaryotes, we expect that our observations and conclusions will prove relevant to other settings involving polarized secretion and efficient compensatory cargo retrieval via CME, such as at presynaptic nerve termini (Saheki and Camilli, 2012).

Materials/Methods

Strains, yeast husbandry, cloning, and plasmids: All yeast strains produced and analyzed in this study can be found in Table S1. All strains were derived from the wild-type diploid DDY1102 and were propagated using standard yeast husbandry techniques (Amberg *et al.*, 2005). Genes encoding C-terminally-tagged fusion proteins were engineered as previously described (Longtine *et al.*, 1998). Genes encoding N-terminally tagged Snc2 fusion proteins were engineered by cloning the genomic *SNC2* open reading frame (ORF) into a pFA6a-XFP backbone to create an in-frame fusion protein. PCR products with homology to the *SNC2* locus were generated from these plasmids, and then transformed into an *snc2Δ* background using previously described techniques (Longtine *et al.*, 1998). The Snc2 V39A M42A double mutant was made at the endogenous *SNC2* locus by introducing the appropriate mutations into the above plasmids using quick-change mutagenesis (Kunkel, 1985). Similarly, the Yap1802 L203S mutant was made by introducing the appropriate mutation into the wild-type gene carried on a pFA6a-GFP backbone, then transforming the resulting PCR product into a *yap1802Δ* strain using previously described techniques (Longtine *et al.*, 1998). All other point mutations were introduced using CRISPR-Cas9 (Anand *et al.*, 2017). All plasmids can be found in Table S2.

Yeast chemical fixation: Yeast strains were grown overnight to mid-log phase (roughly OD 0.2-0.4) in synthetic minimal media and fixed according to previous protocols in 4% paraformaldehyde solution in cytoskeleton buffer (Kaplan and Ewers, 2015).

Live-cell imaging: Yeast strains were grown overnight to mid-log phase (roughly OD 0.2-0.4) in synthetic minimal media lacking tryptophan (containing L-histidine, L-leucine, uracil, L-lysine, adenine, L-methionine, and 2% glucose), then adhered to 8-well imaging chambers (Cellvis C8-1.5H-N) or glass coverslips using 0.2 mg/ml Concanavalin A. *GFP-SNC2 V39A M42A/snc1Δ* strains were grown overnight to mid-log phase in casamino acid media lacking tryptophan (0.17% yeast nitrogen base, 0.5% casamino acid, 0.5% ammonium sulfate, uracil, adenine, and 2% glucose) (Kurokawa *et al.*, 2013). All imaging experiments were repeated a minimum of two times with biological replicates (one mat a and one mat alpha strain) with datapoints consisting either of individual cell intensity traces or individual endocytic events, as per figure legends.

Widefield microscopy was performed using a Nikon Eclipse Ti microscope equipped with a Nikon 100× 1.4 NA Plan Apo VC oil objective and a Neo 5.5 sCMOS camera from Andor Technology. GFP/mScarlet two-color imaging was performed using a Lumencore Spectra X LED light source with a Semrock FF-493/574-Di01 dual-pass dichroic and an FF01-524/628-25 dual-pass excitation filter. Nikon Elements software was used to control the system, and all imaging was done at room temperature (23°C).

Confocal imaging was performed using a Zeiss LSM 900 with Airyscan 2.0 detection equipped with a 60x 1.4 NA oil objective. 1x averaging was used for all acquisitions. Excitation laser wavelengths of 488 nm for GFP and 561 nm for mScarlet were used. Zeiss Zen Blue software was used to control the system, and imaging was performed at 25°C using a temperature-controlled chamber.

NSPARC confocal imaging was performed using a Nikon Eclipse Ti2 microscope equipped with a 60x 1.4 NA Plan Apo λD oil objective and an NSPARC (Nikon Spatial Array Confocal) detector. For the 488 nm laser, an emission range of 503-545 nm was used, and for the 561 nm laser, an emission range of 582-618 nm was used. All data were acquired in Galvo mode with a pinhole size of 18 µM.

Immunoblotting: All protein samples were prepared from cells grown to mid-log phase using trichloroacetic acid (TCA) precipitation (Pedersen and Drubin, 2019). 10% SDS-polyacrylamide gels were run at 100 V and transferred to nitrocellulose membranes at 35 V for 12 hrs. Cells were blocked in 5% milk in PBS, primary antibodies were prepared in PBS with 0.05% milk and 0.1% Tween-20, and secondary antibodies were prepared in PBS with 0.005% milk and 0.1% Tween-20. All incubations occurred at RT for 1 hr with 3 x 5 min PBS washes in between. The following primary antibodies were used in this study: mouse anti-GFP 1:500 (RRID:AB_390913, 11814460001, Roche), mouse anti-V5 1:2,000 (RRID:AB_2792973, R960CUS, Thermo Fisher Scientific), rabbit anti-hexokinase 1:10,000 (RRID:AB_219918, 100-4159, Rockland), and mouse anti-PGK1 1:10,000 (RRID:AB_2532235, 459250, Thermo Fisher Scientific). Immune blots were probed with LICOR fluorophore-conjugated secondary antibodies and imaged on a LICOR Odyssey CLx.

Image and data analysis (code availability): Montages and kymographs were generated using custom scripts in Fiji (NIH) as well as the open-source cell segmentation package CellPose (Stringer *et al.*, 2021; Sun *et al.*, 2024, 2017; Lu and Drubin, 2017). Line trace intensity data for Yap1802 point mutants was analyzed using custom MATLAB scripts. Line traces of medium-budded cells were generated using CellPose, then each intensity profile was interpolated to match the length of the mean trace length. Intensity profiles were averaged at each length and plotted using the MATLAB package plot_areaerrorbar (Martínez-Cagigal, 2024). Moving arrowheads in supplemental movies were added using the Draw_Arrows plugin (Daetwyler *et al.*, 2020). Plots were generated with MATLAB and GraphPad Prism 10. All code is available at https://github.com/DrubinBarnes/Marchando_2024_Snc and https://github.com/geanhu/cme-movie-analysis-2024.

Acknowledgements

We thank all members of the Drubin/Barnes laboratory for their help and support. Yuichiro Iwamoto and Ross Pedersen provided constructive feedback and careful reading of our manuscript. We thank Andrew Wong for his assistance in generating point mutant strains. We are grateful to Constantine Bartolutti and Cyrus Ruediger of the Elçin Ünal/Gloria Brar laboratory for their assistance with CRISPR/Cas9 methodology and for sharing the necessary reagents. In addition, thank you to James Mester for conducting the Nikon NSPARC imaging experiments. This work was supported by NIH grant R35GM118149 (D.G. Drubin).

Figure Legends

FIGURE 1: Spatiotemporal localization of fluorescent protein-tagged Snc1 and Snc2 expressed from their endogenous genomic loci in normal, drug-treated and mutant cells. **A.** Maximum intensity projections of Airyscan confocal z-stacks of fixed yeast cells expressing GFP-Snc1 (with intron removed from the *SNC1* gene) and GFP-Snc2, respectively **B.** Still frames from time-lapse movies of cells expressing GFP-Snc2 and Sla1-mScarlet acquired using a Nikon confocal microscope equipped with an NSPARC detector (see Materials and Methods) **C.** Montages of time-lapse GFP-Snc2 live-cell movies at different stages of cell growth acquired using a Nikon confocal microscope equipped with an NSPARC detector (see Materials and Methods). Time interval between each frame is 1.2 seconds. White arrows in the first and second rows identify unique translating Snc2-positive puncta in daughter and mother cells, respectively **D.** Circumferential kymographs made from 3-minute movies of cells expressing GFP-Snc2 and Sla1-mScarlet in different cell regions and stages of cell growth. Arrows, filled arrows, and barbed arrows denote unique Snc2/Sla1 interaction events in daughter, mother, and unbudded cells, respectively. Temporal resolution is ~0.6 seconds **E.** Still frames from time-lapse Airyscan confocal microscopy movies of wild-type cells expressing GFP-Snc2 and treated with 50 µM CK-666 for 30 minutes, or 2 minutes after washing out the inhibitor (cells in each column are different) **F.** Still frames of widefield time-lapse movies of cells carrying various mutant GFP-Snc2 alleles

FIGURE S1: A. Immunoblot displaying relative levels of V5-AID-tagged Snc1 and Snc2 expressed from their normal promoters at their endogenous loci with anti-hexokinase loading control **B.** Serial dilutions of strains carrying indicated *snc* null mutants or *GFP-SNC2* on YPD **C.** Immunoblot displaying relative levels of GFP-tagged Snc2 and Snc2 V39A M42A mutant **D.** Serial dilutions of wild-type and various *snc* mutant strains on YPD **E.** Immunoblot displaying relative levels of GFP-tagged Yap1802 point mutants **F.** Serial dilutions of strains carrying various Yap1802 point mutations in a *yap1801Δ* background on YPD. **G.** Serial dilutions of control strains for **B**, **D**, and **F**. All immunoblots quantified with ratiometric densitometry

MOVIES S1 and S2: Snc2 interacts with the endocytic machinery in a complex manner. Three-minute movies acquired using a Nikon confocal microscope equipped with an NSPARC detector (see Materials and Methods) of live cells expressing GFP-Snc2 (green) and Sla1-mScarlet (magenta), both from the endogenous promoter and locus from the endogenous promoter and locus in an *snc1Δ* background. Moving arrowheads track distinct Snc2-positive compartments: **Movie S1:** first, a compartment translocating from one location on the plasma membrane to another in a daughter cell, and second, two compartments in the mother cell that move directionally from the cytosol to the bud neck. **Movie S2:** Moving arrowheads track distinct interaction events between GFP-Snc2 and Sla1-mScarlet: first and second at the daughter cell cortex, and third in a mother cell. Acquisition temporal resolution is ~0.6 seconds, playback rate is 27 frames per second. Scale bar is 2 µm

FIGURE 2: Yap1801/2 is recruited to the daughter cortex by Snc1/2 and negatively charged lipids. **A.** Sequence alignment for human CALM and *S. cerevisiae* Yap1802. Red fill indicates

direct matches, and red characters indicate shared residue characteristics (Robert and Gouet, 2014) **B.** Alphafold2 multimer analysis of the ANTH domain of Yap1802 and Snc2, with key residues highlighted in red **C.** Maximum intensity projections from 6-minute widefield microscopy movies of cells expressing various Yap1802 wild-type or point-mutant alleles, 3x PM refers to the K21E K23E L203S triple point mutant **D.** Circumferential kymographs made from 6-minute widefield microscopy movies of Yap1802-GFP point mutants in medium-budded daughter cells. Temporal resolution is 2 seconds **E.** Mean intensities of Yap1802-GFP point mutant line profiles from daughter cell cortexes as in **C.** Right to left, n = 35, 32, 23, 22 **F.** Quantification of Yap1802-GFP point mutant lifetimes **G.** Maximum intensity projections from 3-minute Airyscan confocal microscopy time-lapse movies of cells expressing wild-type Yap1802 or point mutants and mScarlet-Snc2. Temporal resolution of movies was ~3.7 seconds Right to left, n = 127, 129, 106, 97 **H.** Mean intensities of mScarlet-Snc2 line profiles from mother cell cortexes as in **G.** Right to left, n = 17, 15, 17, 14. Groups in **E**, **F**, and **H** were compared using one-way ANOVA. Center and error bars are mean and 95% confidence interval, *** indicates $0.001 > p > 0.0001$, and **** indicates $p < 0.0001$

FIGURE S2: A. GFP line traces of daughter cells as in **C** from wild-type and Yap1802 point mutant maximum intensity projections for the same strains used in **Figure 1C**. **B.** mScarlet-Snc2 line traces from maximum intensity projections of mother cells as in **Figure 1G** expressing Yap1802 wild-type protein or point mutants. For each plot, each trace from individual cells was interpolated to match the mean length of cells in the wild-type cohort. Outlines represent a 95% confidence interval for each point in the trace, annotated microscopy images display examples of individual line traces used

FIGURE 3: **A.** Model for how interaction between synaptobrevin-like v-SNARES Snc1/2 and the CME adaptor proteins Yap1801/2 contributes to CME site initiation and links endocytosis to polarized exocytosis. Cdc42-nucleated actin cables enable directional transport of vesicles toward the daughter bud tip, with fusion near the bud tip assisted by the exocyst vesicle tethering complex. This localized secretion enriches the daughter plasma membrane in Snc1/2, which, in concert with anionic phospholipids, recruit Yap1801/2 to internalize Snc1/2 via CME. **B.** Model for Snc1/2 and anionic phospholipid coincidence detection, enabling robust Yap1801/2 recruitment. Each individual Yap1802 mutant displays defects in recruitment when compared to wild-type, an effect most pronounced in the triple point mutant. Created with BioRender.com.

References

Adams, AE, and Pringle, JR (1984). Relationship of actin and tubulin distribution to bud growth in wild-type and morphogenetic-mutant Saccharomyces cerevisiae. Journal of Cell Biology 98, 934–945.

Amberg, DC, Burke, DJ, and Strathern, JN (2005). Methods in Yeast Genetics: A Cold Spring Harbor Laboratory Course Manual, Cold Spring Harbor, NY: Cold Spring Harbor Laboratory Press.

Anand, R, Memisoglu, G, and Haber, J (2017). Cas9-mediated gene editing in Saccharomyces cerevisiae. Protocol Exchange.

Best, JT, Xu, P, McGuire, JG, Leahy, SN, and Graham, TR (2020). Yeast synaptobrevin, Snc1, engages distinct routes of postendocytic recycling mediated by a sorting nexin, Rcy1-COPI, and retromer. Molecular Biology of the Cell 31, 944–962.

Brach, T, Godlee, C, Moeller-Hansen, I, Boeke, D, and Kaksonen, M (2014). The initiation of clathrin-mediated endocytosis is mechanistically highly flexible. Current Biology 24, 548–554.

Bradford, MK, Whitworth, K, and Wendland, B (2015). Pan1 regulates transitions between stages of clathrin-mediated endocytosis. MBoC 26, 1371–1385.

Burri, L, and Lithgow, T (2004). A Complete Set of SNAREs in Yeast. Traffic 5, 45–52.

Burston, HE, Maldonado-Báez, L, Davey, M, Montpetit, B, Schluter, C, Wendland, B, and Conibear, E (2009). Regulators of yeast endocytosis identified by systematic quantitative analysis. Journal of Cell Biology 185, 1097–1110.

Carroll, SY, Stimpson, HEM, Weinberg, J, Toret, CP, Sun, Y, and Drubin, DG (2012). Analysis of yeast endocytic site formation and maturation through a regulatory transition point. Molecular Biology of the Cell 23, 657–668.

Carroll, SY, Stirling, PC, Stimpson, HEM, Gießelmann, E, Schmitt, MJ, and Drubin, DG (2009). A Yeast Killer Toxin Screen Provides Insights into A/B Toxin Entry, Trafficking, and Killing Mechanisms. Developmental Cell 17, 552–560.

Cocucci, E, Aguet, F, Boulant, S, and Kirchhausen, T (2012). The First Five Seconds in the Life of a Clathrin-Coated Pit. Cell 150, 495–507.

Cortesio, CL, Lewellyn, EB, and Drubin, DG (2015). Control of lipid organization and actin assembly during clathrin-mediated endocytosis by the cytoplasmic tail of the rhomboid protein Rbd2. MBoC 26, 1509–1522.

Daetwyler, S, Modes, CD, and Fiolka, R (2020). Fiji plugin for annotating movies with custom arrows. Biology Open 9, bio056200.

Delattre, S (2023). Igniting New Confocal Imaging Potential – Nikon AX R Series with NSPARC. Microscopy Today 31, 23–27.

Field, C, and Schekman, R (1980). Localized secretion of acid phosphatase reflects the pattern of cell surface growth in saccharomyces cerevisiae. Journal of Cell Biology 86, 123–128.

Ford, MGJ, Pearse, BMF, Higgins, MK, Vallis, Y, Owen, DJ, Gibson, A, Hopkins, CR, Evans, PR, and McMahon, HT (2001). Simultaneous binding of PtdIns (4,5) P2 and clathrin by AP180 in the nucleation of clathrin lattices on membranes. Science 291, 1051–1055.

Godlee, C, and Kaksonen, M (2013). From uncertain beginnings: Initiation mechanisms of clathrin-mediated endocytosis. Journal of Cell Biology 203, 717–725.

Goode, BL, Eskin, JA, and Wendland, B (2015). Actin and Endocytosis in Budding Yeast. Genetics 199, 315–358.

Grote, E, Vlacich, G, Pypaert, M, and Novick, PJ (2000). A snc1 endocytosis mutant: Phenotypic analysis and suppression by overproduction of dihydrosphingosine phosphate lyase. Molecular Biology of the Cell 11, 4051–4065.

Gurunathan, S, Chapman-Shimshoni, D, Trajkovic, S, and Gerst, JE (2000). Yeast exocytic v-SNAREs confer endocytosis. Molecular Biology of the Cell 11, 3629–3643.

Hetrick, B, Han, MS, Helgeson, LA, and Nolen, BJ (2013). Small Molecules CK-666 and CK-869 Inhibit Actin-Related Protein 2/3 Complex by Blocking an Activating Conformational Change. Chemistry & Biology 20, 701–712.

Kaplan, C, and Ewers, H (2015). Optimized sample preparation for single-molecule localization-based superresolution microscopy in yeast. Nature Protocols 2015 10:7 10, 1007–1021.

Katz, L, Hanson, PI, Heuser, JE, and Brennwald, P (1998). Genetic and morphological analyses reveal a critical interaction between the C-termini of two SNARE proteins and a parallel four helical arrangement for the exocytic SNARE complex. The EMBO Journal 17, 6200–6209.

Kreis, TE, Lowe, M, and Pepperkok, R (1995). COPs regulating membrane traffic. Annu Rev Cell Dev Biol 11, 677–706.

Kunkel, TA (1985). Rapid and efficient site-specific mutagenesis without phenotypic selection. Proceedings of the National Academy of Sciences 82, 488–492.

Kurokawa, K, Ishii, M, Suda, Y, Ichihara, A, and Nakano, A (2013). Live Cell Visualization of Golgi Membrane Dynamics by Super-resolution Confocal Live Imaging Microscopy. Methods in Cell Biology 118, 235–242.

Layton, AT, Savage, NS, Howell, AS, Carroll, SY, Drubin, DG, and Lew, DJ (2011). Modeling Vesicle Traffic Reveals Unexpected Consequences for Cdc42p-Mediated Polarity Establishment. Current Biology 21, 184–194.

Lewis, MJ, Nichols, BJ, Prescianotto-Baschong, C, Riezman, H, and Pelham, HRB (2000). Specific Retrieval of the Exocytic SNARE Snc1p from Early Yeast Endosomes. MBoC 11, 23–38.

Lipson, D, Raz, T, Kieu, A, Jones, DR, Giladi, E, Thayer, E, Thompson, JF, Letovsky, S, Milos, P, and Causey, M (2009). Quantification of the yeast transcriptome by single-molecule sequencing. Nature Biotechnology 27, 652–658.

Longtine, MS, Mckenzie III, A, Demarini, DJ, Shah, NG, Wach, A, Brachat, A, Philippsen, P, and Pringle, JR (1998). Additional modules for versatile and economical PCR-based gene deletion and modification in Saccharomyces cerevisiae. Yeast 14, 953–961.

Lu, R, and Drubin, DG (2017). Selection and stabilization of endocytic sites by Ede1, a yeast functional homologue of human Eps15. MBoC 28, 567–575.

Ma, M, and Burd, CG (2019). Retrograde trafficking and quality control of yeast synaptobrevin, Snc1, are conferred by its transmembrane domain. Molecular Biology of the Cell 30, 1729–1742.

Maldonado-Báez, L, Dores, MR, Perkins, EM, Drivas, TG, Hicke, L, and Wendland, B (2008). Interaction between Epsin/Yap180 adaptors and the scaffolds Ede1/Pan1 is required for endocytosis. Molecular Biology of the Cell 19, 2936–2948.

Martin, SG, and Arkowitz, RA (2014). Cell polarization in budding and fission yeasts. FEMS Microbiology Reviews 38, 228–253.

Martínez-Cagigal, V (2024). Shaded area error bar plot. MATLAB Central File Exchange. Available at: https://www.mathworks.com/matlabcentral/fileexchange/58262-shaded-area-error-bar-plot. Accessed May 11, 2024.

Meca, J, Massoni-Laporte, A, Martinez, D, Sartorel, E, Loquet, A, Habenstein, B, and McCusker, D (2019). Avidity-driven polarity establishment via multivalent lipid–GTPase module interactions. The EMBO Journal 38, e99652.

Mei, K, and Guo, W (2018). The exocyst complex. Current Biology 28, R922–R925.

Mei, K, Li, Y, Wang, S, Shao, G, Wang, J, Ding, Y, Luo, G, Yue, P, Liu, J-J, Wang, X, *et al.* (2018). Cryo-EM structure of the exocyst complex. Nat Struct Mol Biol 25, 139–146.

Miller, SE, Sahlender, DA, Graham, SC, Höning, S, Robinson, MS, Peden, AA, and Owen, DJ (2011). The Molecular Basis for the Endocytosis of Small R-SNAREs by the Clathrin Adaptor CALM. Cell 147, 1118–1131.

Mirdita, M, Schütze, K, Moriwaki, Y, Heo, L, Ovchinnikov, S, and Steinegger, M (2022). ColabFold: making protein folding accessible to all. Nat Methods 19, 679–682.

Pashkova, N, Gakhar, L, Yu, L, Schnicker, NJ, Minard, AY, Winistorfer, S, Johnson, IE, and Piper, RC (2021). Anth domains within CALM, HIP1R, and Sla2 recognize ubiquitin internalization signals. eLife 10.

Pedersen, RTA, and Drubin, DG (2019). Type I myosins anchor actin assembly to the plasma membrane during clathrin-mediated endocytosis. Journal of Cell Biology 218, 1138–1147.

Pedersen, RTA, Hassinger, JE, Marchando, P, and Drubin, DG (2020). Spatial regulation of clathrin-mediated endocytosis through position-dependent site maturation. Journal of Cell Biology 219.

Pruyne, D, and Bretscher, A (2000a). Polarization of cell growth in yeast: I. Establishment and maintenance of polarity states. Journal of Cell Science 113, 365–375.

Pruyne, D, and Bretscher, A (2000b). Polarization of cell growth in yeast II. The role of the cortical actin cytoskeleton. Journal of Cell Science 113, 571–585.

Robert, X, and Gouet, P (2014). Deciphering key features in protein structures with the new ENDscript server. Nucleic Acids Research 42, W320–W324.

Saheki, Y, and Camilli, PD (2012). Synaptic Vesicle Endocytosis. Cold Spring Harb Perspect Biol 4, a005645.

Shen, D, Yuan, H, Hutagalung, A, Verma, A, Kümmel, D, Wu, X, Reinisch, K, McNew, JA, and Novick, P (2013). The synaptobrevin homologue Snc2p recruits the exocyst to secretory vesicles by binding to Sec6p. Journal of Cell Biology 202, 509–526.

Stauffer, B, and Powers, T (2015). Target of rapamycin signaling mediates vacuolar fission caused by endoplasmic reticulum stress in Saccharomyces cerevisiae. Mol Biol Cell 26, 4618–4630.

Stringer, C, Wang, T, Michaelos, M, and Pachitariu, M (2021). Cellpose: a generalist algorithm for cellular segmentation. Nat Methods 18, 100–106.

Sun, Y, and Drubin, DG (2012). The functions of anionic phospholipids during clathrin-mediated endocytosis site initiation and vesicle formation. Journal of Cell Science 125, 6157–6165.

Sun, Y, Kaksonen, M, Madden, DT, Schekman, R, and Drubin, DG (2005). Interaction of Sla2p's ANTH domain with PtdIns(4,5)P2 is important for actin-dependent endocytic internalization. Molecular Biology of the Cell 16, 717–730.

Sun, Y, Leong, NT, Jiang, T, Tangara, A, Darzacq, X, and Drubin, DG (2017). Switch-like Arp2/3 activation upon WASP and WIP recruitment to an apparent threshold level by multivalent linker proteins in vivo. eLife 6.

Sun, Y, Leong, NT, Wong, T, and Drubin, DG (2015). A Pan1/End3/Sla1 complex links Arp2/3-mediated actin assembly to sites of clathrin-mediated endocytosis. Molecular Biology of the Cell 26, 3841–3856.

Sun, Y, Yeam, A, Kuo, J, Iwamoto, Y, Hu, G, and Drubin, DG (2024). The conserved protein adaptors CALM/AP180 and FCHo1/2 cooperatively recruit Eps15 to promote the initiation of clathrin-mediated endocytosis in yeast. PLOS Biology 22.

Taylor, MJ, Perrais, D, and Merrifield, CJ (2011). A High Precision Survey of the Molecular Dynamics of Mammalian Clathrin-Mediated Endocytosis. PLOS Biology 9, e1000604.

Toshima, JY, Toshima, J, Kaksonen, M, Martin, AC, King, DS, and Drubin, DG (2006). Spatial dynamics of receptor-mediated endocytic trafficking in budding yeast revealed by using fluorescent alpha-factor derivatives. Proceedings of the National Academy of Sciences of the United States of America 103, 5793–5798.

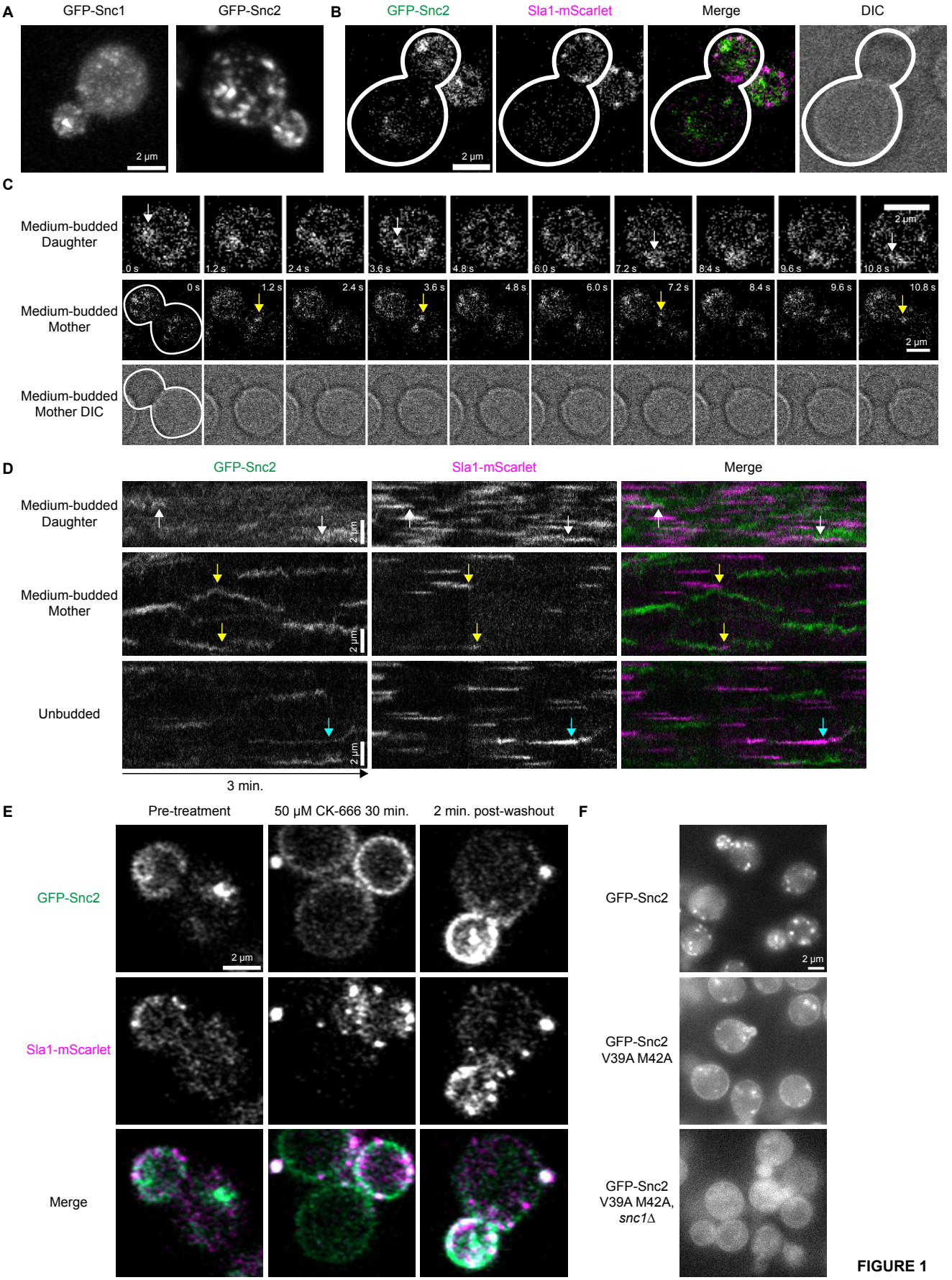
A
GFP-Snc1
GFP-Snc2
2 µm
B
GFP-Snc2
Sla1-mScarlet
Merge
DIC
2 µm
C
Medium-budded Daughter
Medium-budded Mother
Medium-budded Mother DIC
0 s
1.2 s
2.4 s
3.6 s
4.8 s
6.0 s
7.2 s
8.4 s
9.6 s
10.8 s
2 µm
D
GFP-Snc2
Sla1-mScarlet
Merge
Medium-budded Daughter
Medium-budded Mother
Unbudded
2 µm
3 min.
E
Pre-treatment
50 µM CK-666 30 min.
2 min. post-washout
GFP-Snc2
Sla1-mScarlet
Merge
2 µm
F
GFP-Snc2
GFP-Snc2 V39A M42A
GFP-Snc2 V39A M42A, snc1Δ
2 µm

FIGURE 1

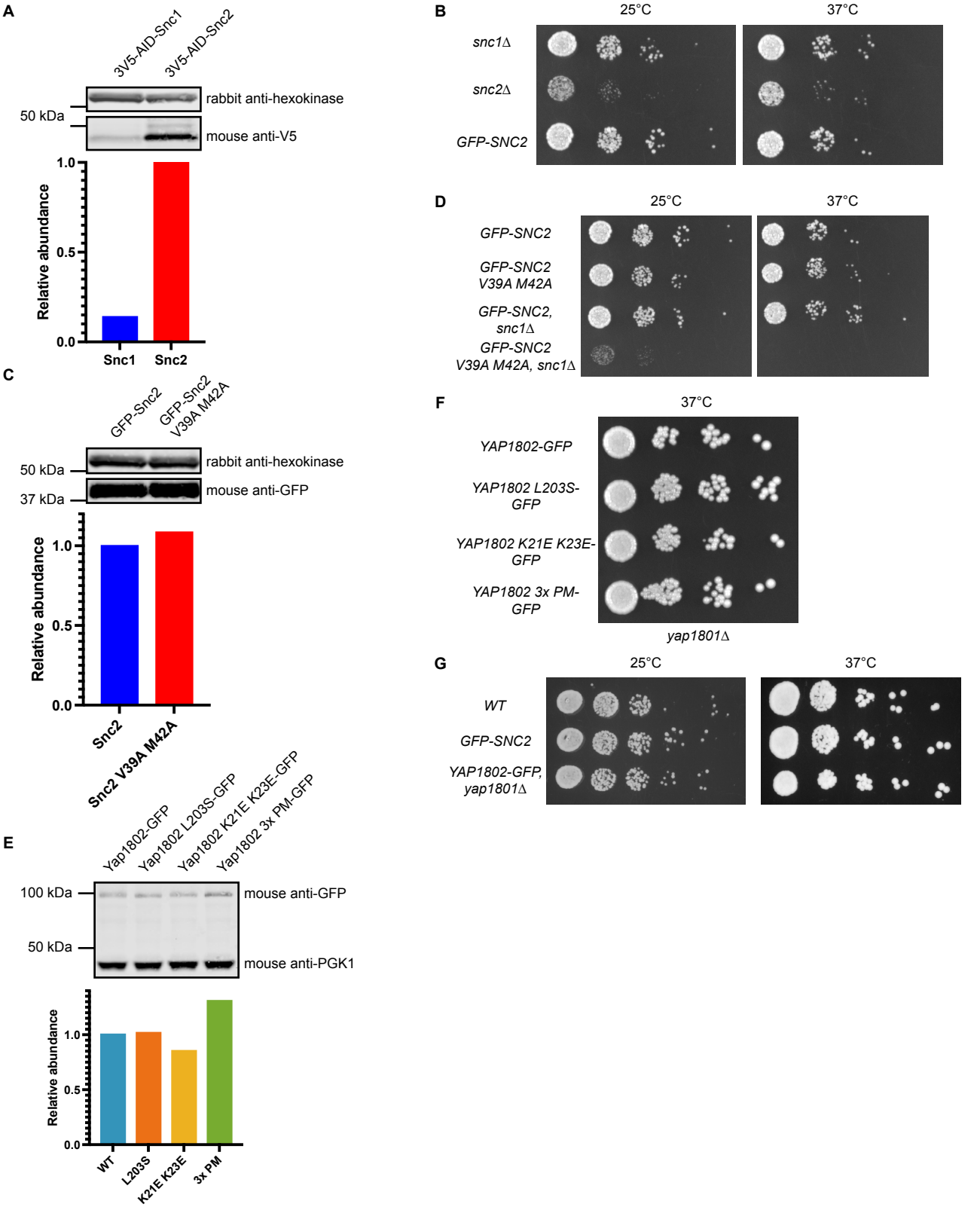
A
3V5-AID-Snc1
3V5-AID-Snc2
50 kDa
rabbit anti-hexokinase
mouse anti-V5
Relative abundance
1.0
0.5
0.0
Snc1
Snc2
B
25°C
37°C
snc1Δ
snc2Δ
GFP-SNC2
C
GFP-Snc2
GFP-Snc2 V39A M42A
50 kDa
37 kDa
rabbit anti-hexokinase
mouse anti-GFP
Relative abundance
1.0
0.5
0.0
Snc2
Snc2 V39A M42A
D
25°C
37°C
GFP-SNC2
GFP-SNC2 V39A M42A
GFP-SNC2, snc1Δ
GFP-SNC2 V39A M42A, snc1Δ
E
Yap1802-GFP
Yap1802 L203S-GFP
Yap1802 K21E K23E-GFP
Yap1802 3x PM-GFP
100 kDa
50 kDa
mouse anti-GFP
mouse anti-PGK1
Relative abundance
1.0
0.5
0.0
WT
L203S
K21E K23E
3x PM
F
37°C
YAP1802-GFP
YAP1802 L203S-GFP
YAP1802 K21E K23E-GFP
YAP1802 3x PM-GFP
yap1801Δ
G
25°C
37°C
WT
GFP-SNC2
YAP1802-GFP, yap1801Δ

FIGURE S1

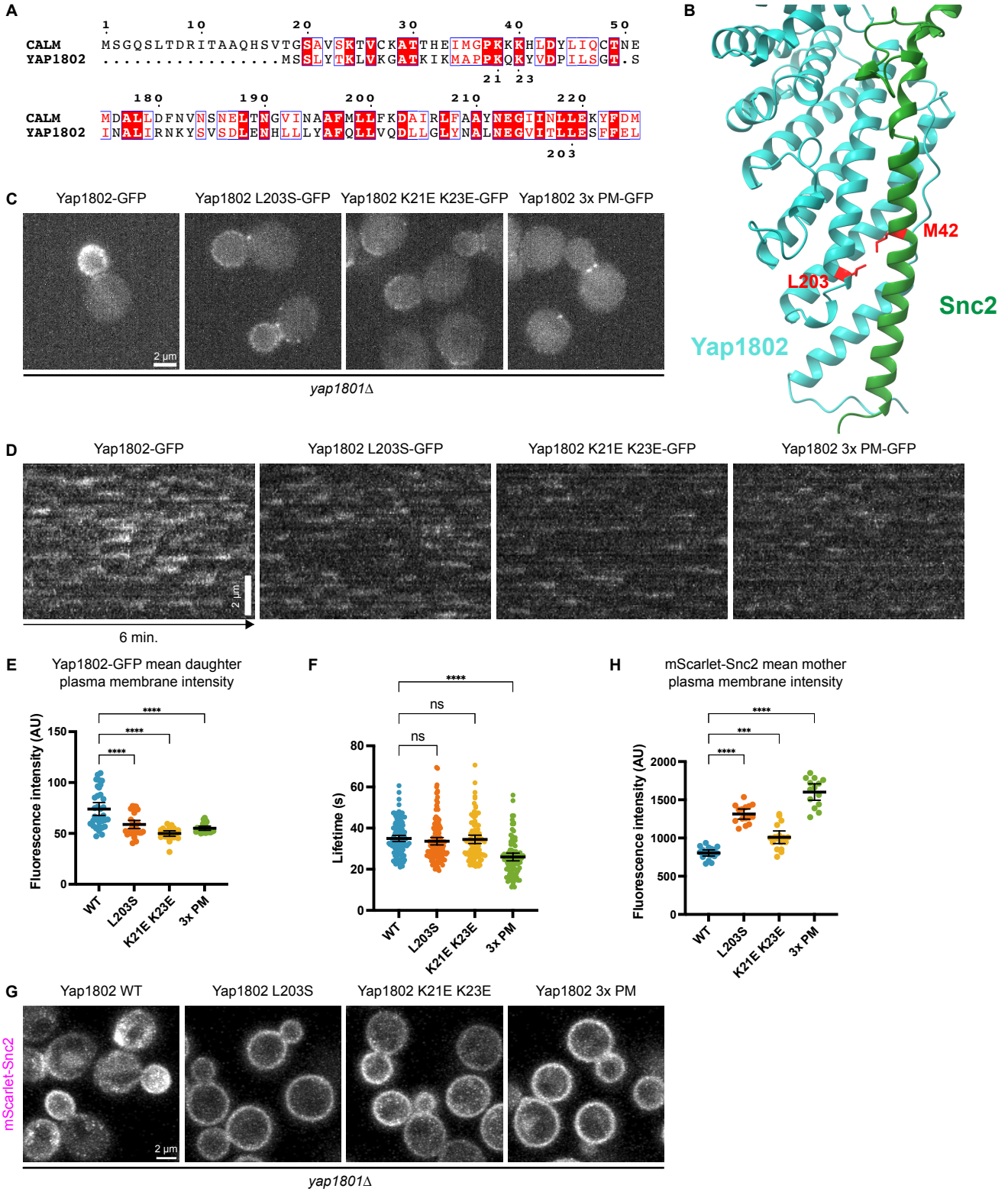
A
CALM
YAP1802
B
M42
L203
Snc2
Yap1802
C
Yap1802-GFP
Yap1802 L203S-GFP
Yap1802 K21E K23E-GFP
Yap1802 3x PM-GFP
2 µm
yap1801Δ
D
Yap1802-GFP
Yap1802 L203S-GFP
Yap1802 K21E K23E-GFP
Yap1802 3x PM-GFP
2 µm
6 min.
E
Yap1802-GFP mean daughter plasma membrane intensity
Fluorescence intensity (AU)
WT
L203S
K21E K23E
3x PM
F
Lifetime (s)
ns
ns
WT
L203S
K21E K23E
3x PM
H
mScarlet-Snc2 mean mother plasma membrane intensity
Fluorescence intensity (AU)
WT
L203S
K21E K23E
3x PM
G
Yap1802 WT
Yap1802 L203S
Yap1802 K21E K23E
Yap1802 3x PM
mScarlet-Snc2
2 µm
yap1801Δ

FIGURE 2

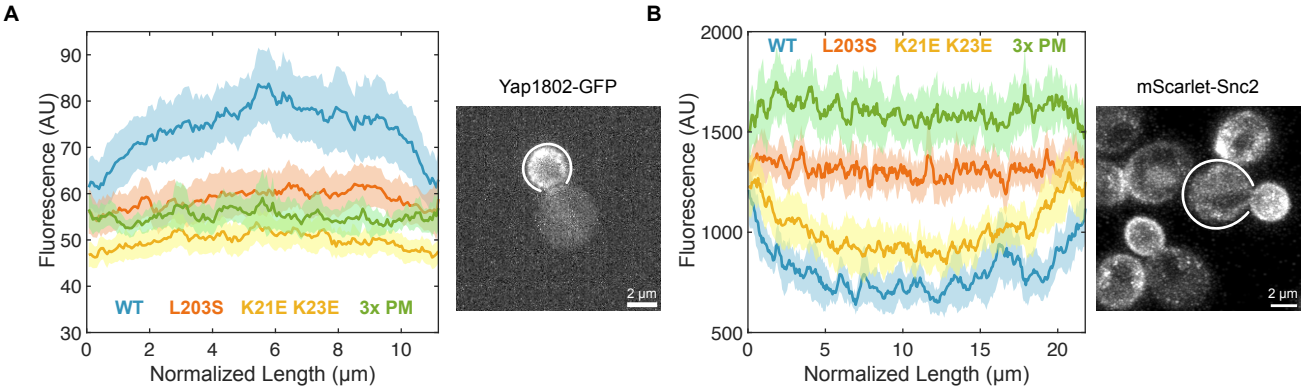
A
Fluorescence (AU)
Normalized Length (μm)
WT
L203S
K21E K23E
3x PM
Yap1802-GFP
2 μm
B
Fluorescence (AU)
Normalized Length (μm)
WT
L203S
K21E K23E
3x PM
mScarlet-Snc2
2 μm

FIGURE S2

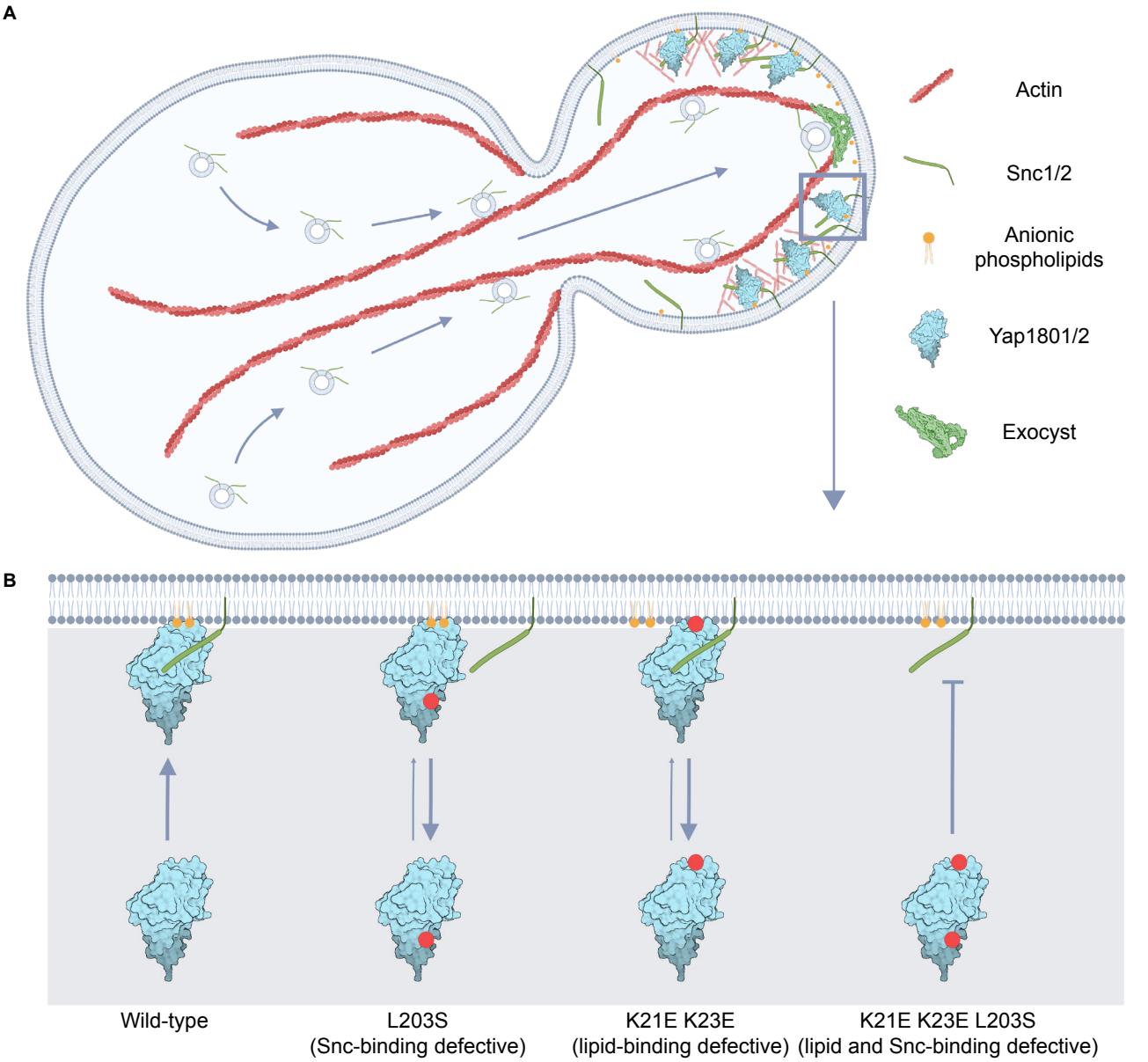
A
Actin
Snc1/2
Anionic phospholipids
Yap1801/2
Exocyst
B
Wild-type
L203S
(Snc-binding defective)
K21E K23E
(lipid-binding defective)
K21E K23E L203S
(lipid and Snc-binding defective)

FIGURE 3